Short-range magnetic order within the multiferroic erythrosiderite mineral $(NH_4)_2FeCl_5 \cdot H_2O$

Adam Berlie,* Hamish Cavaye, and Manh Duc Le
ISIS Neutron and Muon Source, STFC Rutherford Appleton Laboratory, Chilton, Oxfordshire OX11 0QX, United Kingdom

(Received 9 May 2022; revised 13 September 2022; accepted 19 September 2022; published 30 September 2022)

Molecular multiferroics are receiving a large amount of interest, in part due to the ease of synthesis and their potential for tuneability. An important compound within this field is ammonium pentachloroaquaferrate(III), $(NH_4)_2FeCl_5 \cdot H_2O$, which has received a lot of attention due to it having both magnetic and ferroelectric transitions at 7.3 and 6.9 K, respectively. The magnetic structure is complex, with many different exchange pathways; however, to date there has been no consideration of magnetic interactions above the critical temperature. Our paper utilizes muon spin spectroscopy, inelastic neutron scattering and quasielastic neutron scattering (QENS) to show that, as one might expect for these complex magnetic systems, there is indeed evidence for short-range order above 7.3 K and this persists up to ∼15 K. We also highlight the sensitivity of the QENS technique to the magnetic transition and any localized fluctuations.

DOI: 10.1103/PhysRevB.106.104433

I. INTRODUCTION

Multiferroic materials have the potential for some intriguing technological applications [1] and inorganic-organic hybrid materials present some advantages over ceramic/inorganic counterparts [2]. Discovering materials that demonstrate the magnetic and electronic charge coupling required can be challenging as the structure requires a low symmetry, where the inversion symmetry must be broken to allow for electric charge polarization. However in recent years, there have been many successful studies of different multiferroics [3–8].

Almost a decade ago, magneto-electric coupling was shown to exist within the mineral class of erythrosiderite that has the empirical formula, $A_2[FeCl_5(H_2O)]$, where A is either K, Rb, or Cs [9]. Magnetic ordering temperatures of the Fe^{3+} moments were observed between 4 and 15 K for each compound [10,11], where the system was believed to be antiferromagnetic [12,13]. If the alkali metal is swapped for an ammonium cation, to create $(NH_4)_2FeCl_5 \cdot H_2O$, this creates an intriguing material. The structure at higher temperatures has a space group of P_{nma}, with $a = 13.5221(9)$ Å, $b = 9.9305(6)$ Å, $c = 6.9219(6)$ Å, and $\alpha = \beta = \gamma = 90°$, consisting of distorted Fe^{3+} octahedra with isolated $(NH_4)^+$ groups, with the Fe(III) − O bond lying within the ac plane, creating a zigzag pattern of Fe^{3+} interactions. At ∼79 K, there is an order-disorder transition, linked to the freezing of ammonium cation motion [14–16]. There is evidence that the structural phase transition is first order [14], where the crystal structure decreases in symmetry changing from orthorhombic to monoclinic, with space group, $P112_1/a$, $a = 13.5019(6)$ Å, $b = 9.9578(5)$ Å, $c = 6.9049(4)$ Å, and $\alpha = \beta = 90°$ and $\gamma = 90.109(4)°$, as one cools through the phase transition [16].

At low temperatures, the system becomes magnetically ordered at 7.3 K and ferroelectric below 6.8 K, with a strong electric polarization along the a axis and a weaker component, an order of magnitude less, along the b axis and an extremely rich $B - T$ phase diagram [17,18]. The zigzag pattern of Fe^{3+} ions, leads to some complex exchange pathways with five different exchange energies (J_1 to J_5), where at 7.3 K, the system falls into a collinear sinusoidal structure with the magnetic moments along the a direction, mediated by strong spin-lattice coupling [19], with a magnetic propagation vector of $(0,0,k_z)$ where $k_z = 0.2288(4)$ [15]. It is believed that the magnetic ordering then drives the ferroelectricity that emerges at 6.8 K. On cooling through the transition there is a change to an incommensurate cycloidal magnetic structure in the $a - c$ plane, which gives rise to a net electric polarization believed to be due to spin currents induced through the inverse Dzyaloshinskii-Moriya interaction.

The fact that there are two distinct changes in magnetic structure is an interesting point within this material, especially given that the lower temperature transition drives the sample into a ferroelectric state. It has broadly been assumed that in spite of the complex array of different exchange mechanisms (J_1 to J_5), the sample is paramagnetic above 7.3 K. Work by Bai *et al.* [20], shows that J_1 is an order of magnitude larger than J_2 - J_5. Given this, it might suggest that the dominant J_1 exchange could lead to some low-dimensional, or short-range order. Our paper utilizes a combination of techniques to show that above the magnetic transitions, this is indeed the case and there is strong evidence that short-range order persists up to approximately 15 K.

II. EXPERIMENTAL

The sample, $(NH_4)_2FeCl_5 \cdot H_2O$, was synthesised by slow evaporation of an iron (III) chloride and ammonium chloride aqueous solution. Red crystals formed, which could be crushed into a microcrystalline powder for the experiments.

*adam.berlie@stfc.ac.uk

For the deuterated analog used in the inelastic neutron spectroscopy measurement performed on MARI, all synthesis was done using D_2O. The level of deuteration was confirmed using Raman spectroscopy of the O-H and N-H vibrational stretching modes.

Quasielastic neutron spectroscopy (QENS) measurements were performed on the IRIS spectrometer [21]. The sample was loaded into an aluminium sample can and cooled using a closed-cycle refrigerator. The PG002 analyser crystal was used, which provides a resolution of 17.5 μeV and a Q range of 0.42 to 1.85 Å^{-1}.

The inelastic neutron spectroscopy experiment was performed on the MARI spectrometer using a closed-cycle refrigerator to control the sample temperature [22]. The sample was first cooled to 4.3 K and measurements were taken at ≈1 K steps on warming up to 10 K. A Fermi chopper with Gd neutron absorbing slats was run at 100 Hz to define the incident neutron energy of 5 meV, giving an energy resolution of ≈0.2 meV full width at half maximum. For both the INS and QENS, data analysis was performed using Mantid [23].

The muon spin spectroscopy (μSR) experiment [24,25] was performed on the MuSR spectrometer using a He exchange cryostat [26]. Within a μSR experiment, spin polarised positive-muons are implanted within samples and the decay product, a positron, is preferentially emitted along the direction of the spin of the muon at the time of decay; the muon has a half-life of 2.2 μs. The muon couples to the local environment through dipolar coupling or hyperfine interactions. In a static magnetic field, the muon spin will precess at frequency $\nu = \gamma_\mu B$, where γ_μ is the gyromagnetic ratio of the muon and B is the local field. The static field is modulated as electronic fluctuations become present and the relaxation rate of the muon spins provide information on the fluctuation rate of the electronic moments. Given the time scale of the muon half-life, this means any relaxation rate is seen within the MHz time window. Analysis of the muon time spectra was performed using WIMDA [27].

III. EXPERIMENTAL RESULTS

A. Muon spin spectroscopy

The μSR technique is an incredibly effective tool for studying the dynamic character of local electronic fluctuations and static magnetism [24,25]. Previous μSR measurements of the sample have shown that the muon ensemble is sensitive to the magnetic transition and this was extensively studied, where a precession signal is seen below approximately 7.2 K, however, this was lost very quickly as the frequency of the muon spin precession moved outside the time window of the instrument [28].

In order to study the dynamics and the presence of short-range order, our measurements were conducted in a longitudinal field (LF) of 1 kG. The application of the LF is along the initial polarization of the muon. Therefore, the muon spin relaxation rate, λ, is equal to the inverse of the spin-lattice relaxation time with respect to the muon, $1/T_{1\mu}$. The advantage of working within these high LFs is that one is able to decouple the muon from weak phenomena, such as coupling to nuclear moments, so only the contribution from electronic moments is studied.

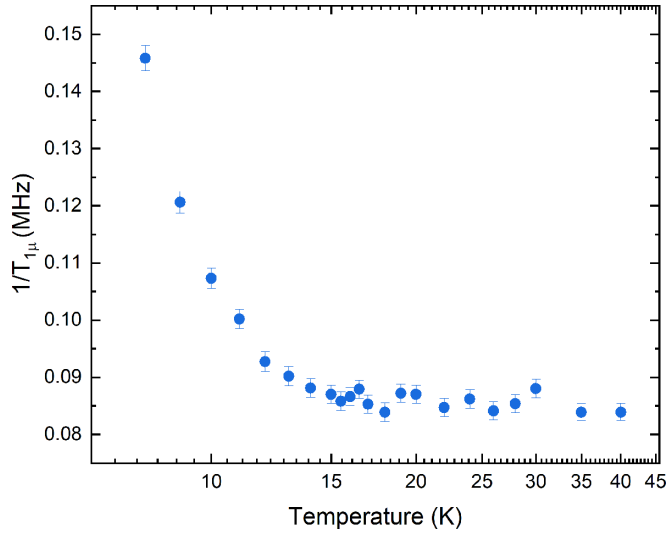

FIG. 1. $1/T_{1\mu}$, the inverse of the spin-lattice relaxation rate of the muon, as a function of temperature collected in an applied longitudinal field of 1 kG.

The results can be seen in Fig. 1, where there is a decrease in $1/T_{1\mu}$ above the magnetic transition. However, this decrease is fairly broad and does not flatten out until above 15 K. Given that the first magnetic transition is at ∼7.2 K, this is significantly higher than one might expect if it was purely electronic fluctuations when approaching the critical region. This broad behavior of $1/T_{1\mu}$ likely points to the presence of short-range order, where the muons are sensitive to dynamic phenomena associated with the onset of local order, as opposed to bulk 3D magnetic order that occurs through the lower temperature transition. Similar results have been observed within other samples where frustration or different exchange pathways lead to a dominant exchange mechanism creating dynamic short-range order [29–33].

B. Inelastic neutron spectroscopy

In order to gain more information on the dynamic state observed within the μSR data, an inelastic neutron spectroscopy experiment was performed on a deuterated powder sample. ^{2}H has a very low incoherent neutron scattering cross section and thus deuteration allows the suppression of vibrational modes in the resulting spectra, meaning that magnetic interactions between the neutrons and sample are dominant. The data were collected between 4 and 10 K in order to follow the data through the magnetic transition, a spectrum taken at 4.3 K can be seen in the supplementary information. Since the magnetic form factor generally drops off quickly with increasing momentum transfer (Q), the data were integrated between $0.3 < Q < 1$ Å^{-1}, allowing one to exclude any contribution of vibrational modes, and the results can be seen in Fig. 2.

Although the data were taken on a microcrystalline powder sample and not a single crystal, the SpinW program [34] was used to simulate the powder averaged data. The constructed model consisted of four different exchange pathways (J_n, where $n = 1, 2, 3, 4$), and is based on the structure and data

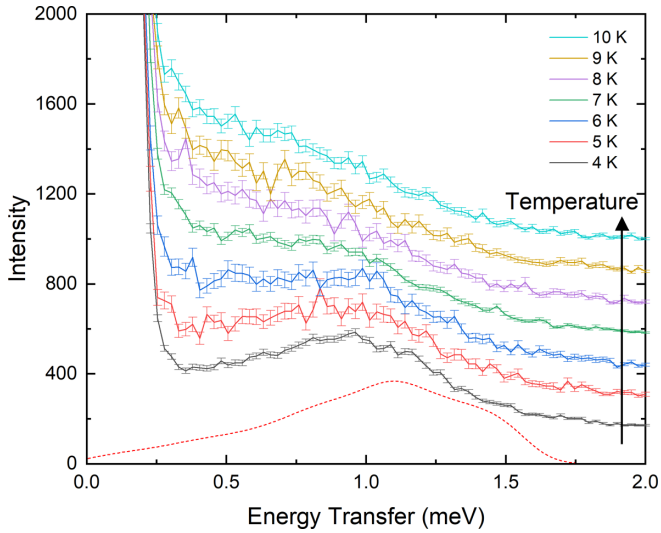

FIG. 2. Inelastic neutron spectra integrated between $0.3 < Q < 1$ Å^{-1}. The data have been offset for clarity with the arrow illustrating the increase in temperature. The dashed line is the simulated (T = 0 K) spectra integrated over Q, as shown within the supplementary information, illustrating broad agreement with the SpinW model and our experimental data.

provided within the paper by Rodríguez-Velamazán *et al.* [15]. For our simulations, the value of k_z was fixed to 0.2288 and to optimize the simulation, so there were imaginary modes, the value of J_4 was allowed to float, resulting in a value of 0.0825 meV or 9.6 K (see Supplemental Material [35] for the convoluted powder spectra and exchange energies used). Good agreement between experiment and theory was achieved, as can be seen in Fig. 2. It is encouraging that the exchange energies (see Supplemental Material [35]) used for the simulation are close to those reported within work by Bai *et al.* [20], in spite of the easy plane term not being included within the simulation. Additionally, it should be noted that only four exchange energies were needed to model the data but this is likely a consequence of working with a powder sample as opposed to a single crystal.

At the lowest temperatures, there is a clear peak at 1 meV due to the spin wave excitations associated with the bulk 3D magnetic order. As the temperature is increased and approaches the transition, the peak begins to broaden. At the transition, there is still evidence of the peak due to spin wave excitation but possibly another quasi-elastic component that enters the energy window.

This clear change at the transition mirrors what is seen within the μSR data, and the fact that there is an onset of a quasielastic component as well as some magnetic excitations, albeit with a broad energy range, is also suggestive of the presence of short-range order above the bulk magnetic transition. In order to further probe the onset of the quasielastic behavior, a QENS experiment was performed.

C. Quasielastic neutron scattering

QENS is sensitive to any motion or disorder that pushes the intensity of the elastic peak into the elastic peak wings (extremely low-energy transfer), such as local paramagnetic fluctuations [36] or even diffuse magnetic moments, where in this case, the broadening of the Bragg peak may also be proportional to the correlation length [37]. However, there is little evidence within the data of Bragg peaks and so it is the incoherent scattering that dominates. This means that the QENS measurements are sensitive to similar dynamic phenomena as the μSR experiment, albeit on a faster time scale (i.e., THz or GHz). All data were collected on warming through the transition.

Since there was no obvious Q variation of the full width half maximum (see Fig. S3 within the Supplemental Material [35]), the raw data were summed over all of Q and although the changes were small, they were measurable. The raw data were fitted using both a delta function convoluted with the resolution function to model the elastic peak and a Lorentzian peak to capture the quasielastic behavior of the sample. Given the low temperatures, molecular motion can be discounted and all of the QENS signal is due to the interaction between the neutron moment and electronic spins within the sample. Figure 3 shows the parameters from the fits to the data. It should be noted that it is commonplace to parameterise the QENS signal using a Lorentzian function [37,38], in our case, the broadening of the Lorentzian is able to model the melting of any magnetic order, where fluctuations are then pushed into the time scale of the measurement and are again able to be modelled using a Lorentzian line shape. Therefore, the temperature dependence of the FWHM, will provide information across the temperature range of interest provided that the magnetic moments are static or fluctuating within the experimental time scale.

As can be seen from Fig. 3(b), the amplitude of the Lorentzian peak increases quickly at the magnetic transition with the amplitude turning over at approximately 10 K and between 15 and 20 K, there may be a slight decrease in the amplitude. This behavior is broadly reproduced by the full width half maximum (FWHM) of the peak [see Fig. 3(c)]. In this case, the FWHM will be related to the fluctuations of the magnetic moments on the Fe(III) ions or any diffuse magnetic scattering. It should be noted that given the values of the FWHM, one is able to observe this within the INS data, however to deconvolute the QENS from the peaks due to the magnetic excitations is challenging. So both data sets can be viewed as complimentary. There is a clear link with the FWHM and the transition at approximately 7.2 K, with a minimum in the data at 9 K. The FWHM then takes off again and plateaus around 15 K. We believe that this is representative of some diffuse, or short-range order, that dissolves above 15 K, where the sample enters the paramagnetic limit.

Further to this, the elastic incoherent structure factor (EISF), summed over all of Q was also calculated from the fits to the data, which is a representation of the change of the elastic component of the single QENS spectra at each temperature compared to the resolution function. There is a clear drop in the EISF as the transition is approached and there is a minimum with an upturn at 15 K. The decrease in EISF is due to some intensity of the elastic line being moved outside of the quasielastic peak, i.e., to higher energy transfer or into a slower/faster time window. The fact that the EISF increases slightly above 15 K, may be because some of this intensity is coming back into the quasielastic peak, likely due to the

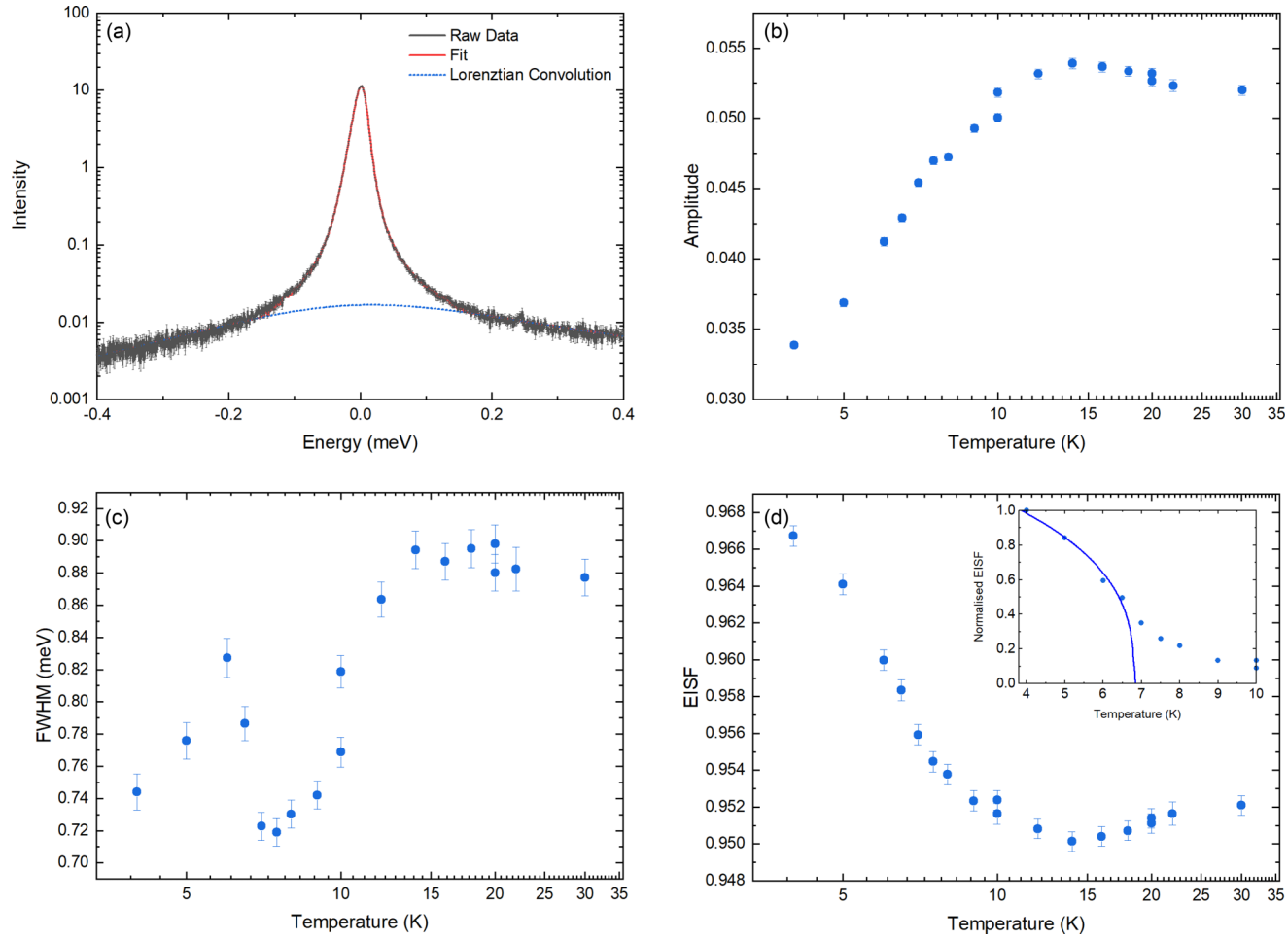

FIG. 3. The temperature dependence of the experimental parameters from fitting the quasielastic neutron spectroscopy data. (a) An example of a fit to the QENS spectra at 9 K, where the Lozrentian component has been illustrated to show the width of the quasielastic process. (b) The amplitude of the QENS peak. (c) The FWHM of the QENS peak related to the increase in quasielastic behavior due to the onset of magnetic fluctuations. (d) The elastic incoherent structure factor (EISF), where the inset shows the normalized EISF at low temperatures with a fit using a critical behavior law. The solid line represents a fit where T_C is fixed at 6.8 K.

break down of short-range order and the sample becoming paramagnetic. Since the EISF is an effective probe of the onset of diffuse scattering or magnetic fluctuations, one might question whether it can be used as a measure of the order parameter. In order to create a representative fit where one can extract meaningful information related to the magnetism the data were normalized where the lowest temperature point is 1 and the minimum value of the EISF is 0. A fit to the normalized EISF, shown in the inset within Fig. 3(d), using a term to extract the critical exponent;

$$EISF = A(1 - T/T_c)^{\beta}, \tag{1}$$

where A is the pre-exponent, T_c is the critical temperature, and β is the critical exponent. A fit was attempted as can be seen in the inset to Fig. 3(d), the solid line represents a fit with T_c fixed at 6.8 K where below this the system is within the noncolinear magnetic phase. In this case, $\beta = 0.34 \pm 0.1$ and $A = 1.34 \pm 0.29$. It is worth highlighting that within these fits the dependency of both the β and A parameters is 0.81, showing that these two parameters are highly coupled. Although within any fit to the temperature dependence of the magnetic order parameter, all parameters within Eq. (1) will have a strong dependency on each other. However, in this case, due to the low number of temperature points, the fit within the inset of Fig. 3(d) should not be taken as gospel but do point to an interesting use of the EISF to model magnetic systems.

With the critical temperature fixed at 6.8 K, this results in a critical exponent of 0.34, in spite of the large error, is close to that expected for a 3D magnet; for a 3D Ising and Heisenberg system one expects β to be 0.32 and 0.36, respectively. However, the fitted critical exponent does not align with that calculated within the paper by Tian *et al.* [19] and although no firm conclusions can be drawn, more work may prove useful to link the behavior of the EISF and the onset of magnetic fluctuations.

IV. DISCUSSION AND CONCLUSIONS

Currently, there is no evidence for any change in the magnetization dynamics at the ferroelectric transition at approximately 6.8 K. However, there are still questions as to whether it is the magnetism that drives the multiferroic transition, or is it a purely structurally driven transition.

As mentioned, previous μSR data [28] focuses on the static component, but our paper has shown that it is likely that short-range order is significant just above the magnetic transition, which is a hallmark of a lower dimensional exchange mechanism dominating the magnetism, as has been suggested within other molecular systems [39,40]. By using QENS, the breakdown of the bulk 3D order can be followed, where the correlated fluctuations collapse into the (quasi)elastic line. Although for a purely paramagnetic system, one would expect the fluctuations to come into the experimental time scale and then move outside as the system becomes motionally narrowed. The rise of the FWHM above the transition is clear evidence that the magnetic fluctuations change and another quasielastic process, namely short-range or diffuse order is present. At 15 K, the magnetic dynamics become motionally narrowed and the structure is quasistatic, where there is no short-range magnetic order or motions associated with the molecular units. It is also noteworthy, that no anomaly is seen at the 6.8 K transition and the trend of all the QENS parameters gives no indication of any distinct structural change. This further supports that it is the magnetism that may drive the multiferrocity. Given the previous work using INS [20] and our data, the simulations point to the J_1 exchange interactions dominating the magnetic behavior, and it is therefore perhaps no surprise that this will lead to short-range order that we have demonstrated in this paper.

In conclusion, using a combination of techniques, it has been possible to demonstrate that there are local interactions that are likely pointing to the existence of dynamic magnetic short-range order within the molecular multiferroic, $(NH_4)_2[FeCl_5(H_2O)]$. All previous studies assumed that above 7.3 K, the sample was simply paramagnetic, however, we have shown this is not the case. Additional work could be performed to understand whether application of higher magnetic fields can suppress this short-range order. Given the dominant antiferromagnetic interaction of J_1, which forms zigzag patterns within the $a-b$ plane, the short-range order may be dominated by 1D correlations, however again, more work is needed to confirm this.

ACKNOWLEDGMENTS

We would like to thank the ISIS Neutron and Muon Source for access to muon spin spectroscopy and neutron spectroscopy beam time. We would also like to thank Dr. Ian Terry, Durham University for fruitful discussions about the data.

[1] M. M. Vopson, Crit. Rev. Solid State Mater. Sci. **40**, 223 (2015).
[2] X.-L. Liu, D. Li, H.-X. Zhao, X.-W. Dong, L.-S. Long, and L.-S. Zheng, Adv. Mater. **33**, 2004542 (2021).
[3] E. Pardo, C. Train, H. Liu, L.-M. Chamoreau, B. Dkhil, K. Boubekeur, F. Lloret, K. Nakatani, H. Tokoro, S.-I. Ohkoshi, and M. Verdaguer, Angew. Chem. Int. Ed. **51**, 8356 (2012).
[4] N. A. Spaldin and R. Ramesh, Nat. Mater. **18**, 203 (2019).
[5] Z. Qiu, D. Hou, J. Barker, K. Yamamoto, O. Gomonay, and E. Saitoh, Nat. Mater. **17**, 577 (2018).
[6] P. Lunkenheimer, J. Muller, S. Krohns, F. Schrettle, A. Loidl, B. Hartman, R. Rommel, M. de Souza, C. Hotta, J. A. Schlueter, and M. Lang, Nat. Mater. **11**, 755 (2012).
[7] G. Giovannetti, S. Kumar, A. Stroppa, J. van den Brink, and S. Picozzi, Phys. Rev. Lett. **103**, 266401 (2009).
[8] M. Fiebig, T. Lottermoser, D. Meier, and M. Trassin, Nat. Rev. Mater. **1**, 16046 (2016).
[9] M. Ackermann, T. Lorenz, P. Becker, and L. Boharty, J. Phys.: Condens. Matter **26**, 506002 (2014).
[10] R. L. Carlin, S. N. Bhatia, and C. J. O'Connor, J. Am. Chem. Soc. **99**, 7728 (1977).
[11] J. N. McElearney and S. Merchant, Inorg. Chem. **17**, 1207 (1978).
[12] M. Gabas, F. Palaciot, J. Rodríguez-Carvajal, and D. Visser, J. Phys.: Condens. Matter **7**, 4725 (1995).
[13] J. Campo, J. Luzón, F. Palacio, G. J. McIntyre, A. Millán, and A. R. Wildes, Phys. Rev. B **78**, 054415 (2008).
[14] M. Ackermann, D. Brüning, T. Lorenz, P. Becker, and L. Bohatý, New J. Phys. **15**, 123001 (2013).
[15] J. A. Rodríguez-Velamazán, O. Fabelo, A. Millán, J. Campo, R. D. Johnson, and L. Chapon, Sci. Rep. **5**, 14475 (2015).
[16] D. Brüning, T. Fröhlich, M. Langenbach, T. Leich, M. Meven, P. Becker, L. Bohatý, M. Grüninger, M. Braden, and T. Lorenz, Phys. Rev. B **102**, 054413 (2020).
[17] A. J. Clune, J. Nam, M. Lee, K. D. Hughey, W. Tian, J. A. Fernandez-Baca, R. Fishman, J. Singleton, J. H. Lee, and J. L. Musfeldt, npj Quantum Mater. **4**, 44 (2019).
[18] S. Li and R. S. Fishman, Phys. Rev. B **104**, L060407 (2021).
[19] W. Tian, H. Cao, J. Wang, F. Ye, M. Matsuda, J.-Q. Yan, Y. Liu, V. O. Garlea, H. K. Agrawal, B. C. Chakoumakos, B. C. Sales, R. S. Fishman, and J. A. Fernandez-Baca, Phys. Rev. B **94**, 214405 (2016).
[20] X. Bai, R. S. Fishman, G. Sala, D. M. Pajerowski, V. O. Garlea, T. Hong, M. Lee, J. A. Fernandez-Baca, H. Cao, and W. Tian, Phys. Rev. B **103**, 224411 (2021).
[21] Data can be found at https://doi.org/10.5286/ISIS.E.RB2010779.
[22] Data can be found at https://doi.org/10.5286/ISIS.E.RB2000275.
[23] O. Arnold, J. C. Bilheux, J. M. Borreguero, A. Buts, S. I. Campbell, L. Chapon, M. Doucet, N. Draper, R. Fer-raz Leal, M. A. Gigg *et al.*, Nucl. Instrum. Methods Phys. Res. Sect. A **764**, 156 (2014).
[24] A. D. Hillier, S. J. Blundell, I. McKenzie, I. Umegaki, L. Shu, J. A. Wright, T. Prokscha, F. Bert, K. Shimomura, A. Berlie *et al.*, Nat. Rev. Methods Primers **2**, 4 (2022).
[25] S. J. Blundell, R. De Renzi, T. Lancaster, and F. L. Pratt, *Muon Spectroscopy: An Introduction* (Oxford University Press, Oxford, 2021).
[26] Data can be found at https://doi.org/10.5286/ISIS.E.RB2090044.
[27] F. L. Pratt, Phys. B: Condens. Matter **289-290**, 710 (2000).
[28] M. Attenborough, I. Hall, O. Nikolov, and S. R. Brown, Hyperfine Interact. **108**, 435 (1997).
[29] J. A. Hodges, P. Bonville, A. Forget, A. Yaouanc, P. Dalmas de Réotier, G. André, M. Rams, K. Królas, C. Ritter, P. C. M. Gubbens, C. T. Kaiser, P. J. C. King, and C. Baines, Phys. Rev. Lett. **88**, 077204 (2002).

[30] H. Yamauchi, D. Puspita Sari, I. Watanabe, Y. Yasui, L.-J. Chang, K. Kondo, T. U. Ito, M. Ishikado, M. Hagihara, M. D. Frontzek *et al.*, Commun. Mater. **1**, 43 (2020).

[31] R. Dally, T. Hogan, A. Amato, H. Luetkens, C. Baines, J. Rodriguez-Rivera, M. J. Graf, and S. D. Wilson, Phys. Rev. Lett. **113**, 247601 (2014).

[32] P. J. Baker, T. Lancaster, S. J. Blundell, M. L. Brooks, W. Hayes, D. Prabhakaran, and F. L. Pratt, Phys. Rev. B **72**, 104414 (2005).

[33] A. Yaouanc and P. Dalmas De Réotier, *Muon Spin Rotation, Relaxation and Resonance; Applications to Condensed Matter* (Oxford University Press, Oxford, 2011).

[34] S. Toth and B. Lake, J. Phys.: Condens. Matter **27**, 166002 (2015).

[35] See Supplemental Material at http://link.aps.org/supplemental/10.1103/PhysRevB.106.104433 for raw INS spectra at 4.3 K; a simulation of spectra at $T = 0$ K using SpinW; a table with exchange energies used in model; and QENS spectra at 10 K at different values of Q.

[36] J. Gunasekera, L. Harriger, T. Heitmann, A. Dahal, H. Knoll, and D. K. Singh, Phys. Rev. B **91**, 241103(R) (2015).

[37] A. T. Boothroyd, *Principles of Neutron Scattering from Condensed Matter* (Oxford University Press, Oxford, 2020).

[38] M. T. F. Telling, *A Practical Guide to Quasi-Elastic Neutron Scattering* (Royal Society of Chemistry, London, 2020).

[39] J. L. Manson, T. Lancaster, L. C. Chapon, S. J. Blundell, J. A. Schlueter, M. L. Brooks, F. L. Pratt, C. L. Nygren, and J. S. Qualls, Inorg. Chem. **44**, 989 (2005).

[40] J. L. Manson, M. M. Conner, J. A. Schlueter, A. C. McConnell, H. I. Southerland, I. Malfant, T. Lancaster, S. J. Blundell, M. L. Brooks, F. L. Pratt *et al.*, Chem. Mater. **20**, 7408 (2008).